Desalination 330 (2013) 35–41

Contents lists available at ScienceDirect

Desalination

journal homepage: www.elsevier.com/locate/desal

Energy consumption in membrane capacitive deionization for different water recoveries and flow rates, and comparison with reverse osmosis

R. Zhao [a,b], S. Porada [b,c], P.M. Biesheuvel [a,b], A. van der Wal [a,*]

[a] Department of Environmental Technology, Wageningen University, Bornse Weilanden 9, 6708 WG, Wageningen, The Netherlands
[b] Wetsus, Centre of Excellence for Sustainable Water Technology, Agora 1, 8934 CJ Leeuwarden, The Netherlands
[c] Department of Polymers and Carbon Materials, Faculty of Chemistry, Wroclaw University of Technology, Wybrzeze Wyspianskiego 27, 50-370 Wroclaw, Poland

HIGHLIGHTS

- New method of data analysis for (membrane) capacitive deionization is presented.
- Energy consumption and energy recovery (during discharge) of MCDI is analyzed.
- Constant current operational mode for MCDI results in a stable effluent salt concentration.
- Membrane capacitive deionization is compared with reverse osmosis.

ARTICLE INFO

Article history:
Received 22 June 2013
Received in revised form 8 August 2013
Accepted 9 August 2013
Available online xxxx

Keywords:
Membrane capacitive deionization
Energy recovery
Reverse osmosis
Water recovery

ABSTRACT

Membrane capacitive deionization (MCDI) is a non-faradaic, capacitive technique for desalinating brackish water by adsorbing ions in charged porous electrodes. To compete with reverse osmosis, the specific energy consumption of MCDI needs to be reduced to less than 1 kWh per m^3 of freshwater produced. In order to investigate the energy consumption of MCDI, we present here the energy consumption, and the fraction of energy that can be recovered during the ion desorption step of MCDI, as a function of influent concentration, water flow rate and water recovery. Furthermore, the energy consumption of MCDI based on experimental data of our lab-scale system is compared with literature data of reverse osmosis. Comparing with literature data for energy consumption in reverse osmosis, we find that for feed water with salinity lower than 60 mM, to obtain freshwater of ~1 g TDS/L, MCDI can be more energy efficient.

1. Introduction

Freshwater scarcity is one of the most severe problems of our time. Although the total water storage on the earth is 1.4 Gm^3, usable freshwater including rivers, lakes and ground water occupies only a tiny fraction of 0.65% of the total water storage [1]. Because of population growth and ongoing urbanization, over two thirds of the human population will be facing freshwater scarcity in the near future to a smaller or larger extent [2]. Therefore, new freshwater sources have to be made available by desalination of seawater or brackish water. For seawater desalination, many well-proven technologies exist for decades, such as reverse osmosis (RO), electrodialysis (ED), multiple effect distillation (MED) and multistage flash desalination (MSF) [3]. However, for brackish water desalination, the above-mentioned technologies may become less favorable in terms of energy efficiency. Innovative techniques, such as forward osmosis [4], ion concentration polarization in microporous media [5], and capacitive deionization, have been advanced together with the use of renewable energy sources (solar, wind, etc.) in order to provide energy saving solutions [6]. In this paper, we will focus on capacitive deionization (CDI), a non-faradaic process which adsorbs salt ions based on capacitive porous electrodes [7–19].

A capacitive deionization cell consists of two porous electrodes placed face-to-face, and a flow channel in between for water to pass through. When charging the electrodes with an external DC energy source (battery, solar panel, etc.), the ions in the water stream will be adsorbed into the micropores of the electrodes; and when discharging the electrodes by short-circuiting or reducing the voltage across the electrodes, the adsorbed ions will be released back into the flow channel. Those two steps are called ion adsorption step and ion desorption step. By placing a cation exchange membrane in front of the cathode and an anion exchange membrane in front of the anode, a membrane

* Corresponding author at: Department of Environmental Technology, Wageningen University, Bornse Weilanden 9, 6708 WG, Wageningen, The Netherlands. Tel.: +31 (0) 317 48 33 39.
E-mail address: bert.vanderwal@wur.nl (A. van der Wal).

0011-9164/$ – see front matter © 2013 Elsevier B.V. All rights reserved.
http://dx.doi.org/10.1016/j.desal.2013.08.017

capacitive deionization (MCDI) cell, a modification of the CDI cell, is thus constructed [7,20–25] (see Fig. 1). In MCDI, during the salt removal step, the salt concentration in the macropores of the electrode (on one side of the membrane) becomes higher than that in the spacer channel which is on the other side of the membrane [7]. Therefore, because of the use of ion exchange membranes (IEMs) in MCDI, more ions can be adsorbed per gram of total electrode mass, and in addition, less energy is consumed than in CDI [26]. It is also demonstrated that in MCDI, the energy consumption is about the same in both constant current (CC) and constant potential (CV) modes [26]. In the CC mode, a constant current is applied during salt removal leading to a constant salt effluent concentration. During desorption, either the cell is short-circuited (ZVD mode) or the current is reversed (RCD mode) [26]. In the RCD mode, a constant current is applied during the adsorption step for a given time, and also during the desorption step, a constant current in the opposite direction is applied until the resulting cell voltage decreases to zero.

Because the energy consumption of CDI is reported to be lower than that of RO [27–30] in certain cases, and because the energy consumption of MCDI is lower again than that of CDI [26], it is worthwhile to investigate in more detail the energy consumption of MCDI under different conditions and to compare the energy consumption of MCDI with RO. In this paper, we will illustrate how we compare energy consumption per ion removed, as a function of influent salt concentrations, by varying the electrical current and water flow rate, in the MCDI-CC-RCD operational mode exclusively. Note that in the ion desorption step, it is possible to recover energy due to the release of stored charge. Długołęcki and Van der Wal [31] claim that up to 83% of the energy invested during the ion adsorption step can be recovered during the ion release step by using the CC mode. Similarly, Demirer et al. [32] found a 63% energy recovery by using the CV mode. Note that these high numbers are obtained under rather relaxed conditions, in other words, high salt removal efficiency is not aimed for. In this work, we present results for the energy recovery as a function of water recovery and flow rate. For all the experiments in section 3.1 and section 3.2, the salt removal efficiency is set to 50% (all solutions are desalinated to half of their initial salt concentration, except for results presented in Fig. 7), which is a much higher number than in refs. [31,32]. We also compare the energy consumption of MCDI with that of RO, when freshwater is produced for different influent salt concentrations.

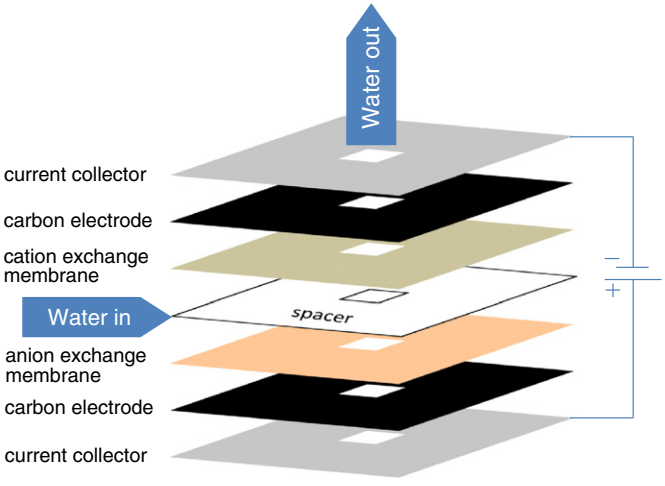

Fig. 1. Schematic view of a membrane capacitive deionization (MCDI) cell. Influenced by the electrical voltage difference between the two electrodes, anions present in the water flowing through the spacer channel migrate through the anion-exchange membrane and are stored inside the adjacent porous electrode; simultaneously, cations are stored in the opposite electrode.

2. Materials and Methods

2.1. Materials and layout of the setup

Experimental details of the MCDI stack are elaborated in this section. Materials used are graphite current collectors (Cixi Sealing Spacer Material Factory, Ningbo City, China, thickness $\delta = 250$ μm), porous carbon electrodes (Materials and Methods, PACMM™ 203, Irvine, CA, USA, $\delta_e = 383$ μm), anion and cation-exchange membranes (Neosepta AMX, $\delta_{mem} = 140$ μm, and Neosepta CMX, $\delta_{mem} = 170$ μm, Tokuyama, Japan) and a polymer spacer (Glass fibre prefilter, Millipore, Ireland, $\delta_{sp} = 250$ μm). In Sections 3.1 and 3.2, we use 8 cells (16 electrodes). The total dry electrode mass is 11.8 g. In Section 3.3, 13 cells (26 electrodes) are used, and the total dry mass is 19.0 g. After assembly, all layers in the stack are compressed and placed in a PTFE housing. The salt solution (NaCl) flows from all four sides of the stack into the square 6×6 cm^2 spacer channel of each of the cells then leaves from a hole (1.5×1.5 cm^2) in the middle of each cell (Fig. 1). The effluent conductivity is measured by an inline conductivity meter and is converted into the salt concentration according to a conductivity–concentration calibration curve. The stack is fed from a 10-L vessel, and the effluent is recycled. The electrical current and voltage across the cell are applied and measured by a potentiostat (Iviumstat standard, Ivium Technologies, The Netherlands). All experiments are performed in the single-pass mode, which is described in ref. [7].

2.2. Data analysis

The salt adsorption and charge in an MCDI-cycle can be derived from the data of effluent salt concentration and electrical current versus time, following the procedure as explained in Ref. [7]. For salt adsorption, the concentration difference between the inflow and the outflow is integrated over time and multiplied with the water flow rate. In the classical mode, this integration is done from the moment a voltage or a current is applied till the moment that the voltage is reduced, or the current is reversed. This period defines the ion adsorption step. For charge, the current is integrated over time during this same period. In addition, energy consumption is also calculated based on integrating the power (product of cell voltage V_{cell} and applied current I) during the ion adsorption step, used in Ref. [26]. In this procedure, the beginning and the end of a cycle is the moment when a step change of current or voltage occurs. If the desorption time is not long enough for complete ion release (less than ~500 s), after dynamic equilibrium (previously defined as dynamic steady state, see refs. [26,33]) is reached, normally there will be a systematic delay of the salt adsorption/desorption as a function of time compared to the current/voltage change, to be discussed later. Because of the delay, the data analysis procedure can be further modified in order to reflect the "real" salt adsorption and energy consumption.

To begin with, we will present the analysis of data under the dynamic equilibrium (DE) condition in detail for salt adsorption and energy consumption. Under the DE condition, the salt removal during the ion adsorption step is equal to the release of salt in the ion desorption step, and equal to the salt removal and release in further cycles. This condition is known as salt balance, and likewise, charge balance is also achieved [26], which means that all charge transferred to the electrodes during ion adsorption step is released again during ion desorption step. In DE, we have salt balance and charge balance. Instead, during the first 1 or 2 cycles of a new series, there can be a deviation with more charge or salt adsorbed than desorbed, see Fig. 2 very left. Note that in this work we only analyze data obtained under DE conditions. Fig. 2 shows an example of cycles of (a) effluent salt concentration, (b) current and (c) cell voltage obtained during the experiment, where the influent is 40 mM NaCl solution and the total water flow rate is 30 mL/min for a stack consisting of 8 cells. During the adsorption step, an electrical current (1 A) is applied to the entire stack (8 cells) for 100 s, and during the

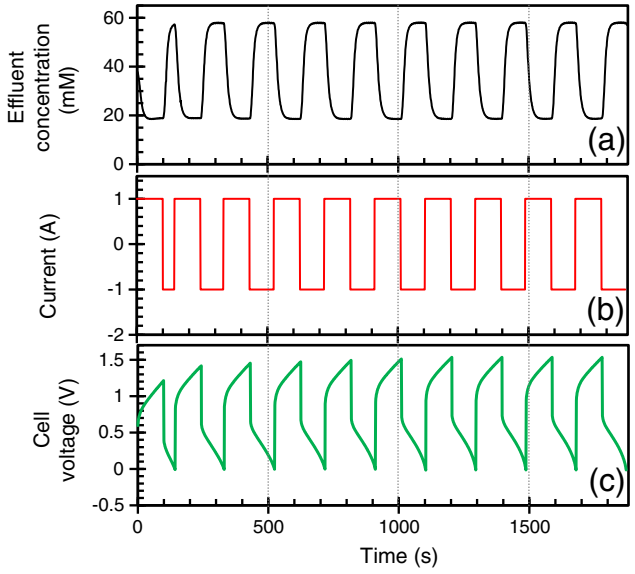

Fig. 2. Experimental results of (a) effluent concentration, (b) current and (c) cell voltage as function of time. Influent: 40 mM NaCl. During the adsorption step, an electrical current of 1 A was applied for 100 seconds, after that the current during the ion-release step was controlled at −1 A until the cell voltage dropped back to 0 V for each cycle. In total, a series of 10 cycles is shown, and dynamic equilibrium was reached after the 3rd cycle.

desorption step, −1 A is applied until the cell voltage drops to V_{cell} = 0 V. Note that 1 A translates to a current density of 37 A/m^2 membrane.

Taking the 7th cycle that is under the DE condition in Fig. 2 as an example, see Fig. 3, once the electrical current is applied, the cycle starts. This is also the beginning of the integration for both salt adsorption and charge in the classical data analysis as discussed above [26]. Yet at that moment, the effluent concentration is still higher than the influent concentration. It takes a few seconds for the effluent concentration to become lower than the influent concentration, and only then the 'real' adsorption step starts. This "real" beginning of the adsorption step has a brief and systematic delay in comparison to the moment when the electrical current is applied, and this delay can be found in all cycles under the DE condition.

Similarly, for desorption, when the current is reversed from 1 to −1 A (adsorption ends, desorption starts), it takes the effluent concentration again a few seconds to exceed the influent concentration, and also when the current is reversed to 1 A again, the effluent concentration does not drop below the influent concentration immediately, but after several seconds. This system delay, which occurs every time when the electrical current is changed, is mainly caused by the continuous mixing of just produced freshwater with untreated water in the spacer channel and in the additional volume present in the housing [34]. Hence, to show the real salt adsorption, instead of integrating the salt concentration difference between influent and effluent from the moment in time when the current is applied till the current is reversed, we integrate over the time period from point A (Fig. 3a), where the effluent concentration intersects the influent concentration, to the second intersection, point B (Fig. 3a). Similarly for the salt desorption, we integrate from intersection B to intersection C (Fig. 3a). According to the new data analysis method, the salt adsorption period is $\Delta t_{A\to B}$ and the salt desorption period is $\Delta t_{B\to C}$, and thus the water recovery (WR) is given by WR = $\Delta t_{A\to B}/\Delta t_{A\to C}$.

Fig. 3b shows the electrical current density and the cell voltage as function of time, for the 7th cycle in the series presented in Fig. 2. To display the power (W) as function of time as shown in Fig. 3c, the current (I) and the corresponding cell voltage at every moment in time are multiplied. The energy consumption of an entire cycle can be computed by integrating the power over time for the whole cycle. During the adsorption step, the current (I) and the voltage (V) have the same sign (+), and thus the power (W), has always a positive value, implying ion adsorption costs energy. In our previous work [26], we only took the adsorption step into account for the energy calculation. However, during the ion desorption step, ions are released spontaneously, thereby creating a negative current, while the cell voltage is still positive, which results in a negative power, meaning that one can recover energy during this ion release step, e.g., by powering another (M)CDI system or a rechargeable battery. In the new method of analysis, we assume that all the released energy during the desorption step can be fully recovered. Thus, the total energy consumption, E_{tot}, is equal to the sum of the energy consumption during the ion adsorption step, E_{ads}, and the energy recovered during the ion desorption step, E_{des}, given by

$$E_{tot} = E_{ads} + E_{des}, \tag{1}$$

$$E_{ads} = I_{ads} \cdot \int_0^{t_{ads}} V \cdot dt, \tag{2}$$

$$E_{des} = I_{des} \cdot \int_{t_{ads}}^{t_{cycle}} V \cdot dt, \tag{3}$$

where t_{cycle} and t_{ads} represent the end time of a total cycle and of the ion adsorption step (given that a cycle starts from time zero), and I_{ads} and I_{des} are adsorption current (positive) and desorption current (negative), respectively. The energy recovery is defined as the ratio of the absolute value of energy recovered during the ion desorption step to the

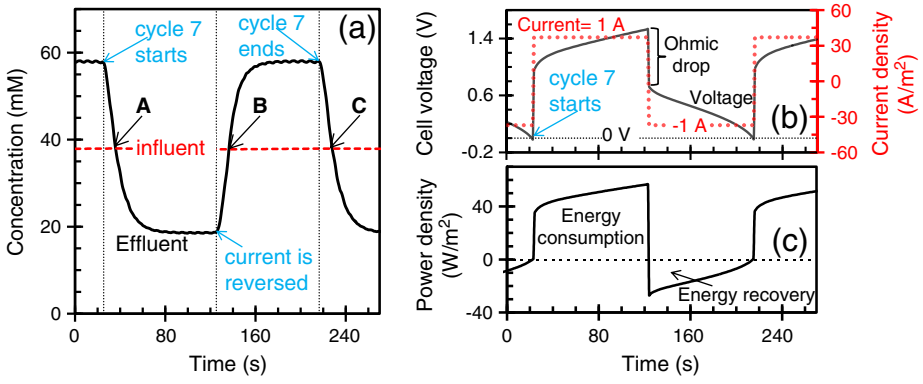

Fig. 3. Example data for MCDI operation at constant current (CC). (a) Influent/effluent concentration (mM) as function of time. Dashed line: influent concentration; solid line: effluent concentration. (b) Cell voltage (V) and current density (A/m^2) as function of time. Dashed line: current density; solid line: voltage. (c) Power density (W/m^2), which is the product of current and voltage as function of time.

Table 1
Comparison of salt adsorption, dynamic charge efficiency, and energy consumption per ion removed for the MCDI-CC-RCD data point at 200 mM in Fig. 3c of ref. [24], by two methods of analysis.

	Ref. [24]	This paper
Salt adsorption (mmol/g)	0.108	0.112
Dynamic charge efficiency	0.75	0.78
Energy consumption per ion removed (kT)	33	24

energy consumption during the ion adsorption step, which is equal to $|E_{des}|/E_{ads}$.

Using the new data analysis approach, we re-analysed as an example one data point at 200 mM (MCDI-CC-RCD) in Fig. 3c in ref. [26]. Table 1 shows that with the new analysis method, we are able to "increase" the salt adsorption and the dynamic charge efficiency slightly, and "decrease" the energy consumption per ion removed significantly. Apparently, when presenting data of CDI performance especially for energy, it is imperative to clearly define the method used.

2.3. Experimental details

In this section, we present the experimental details for the data to be discussed in Section 3. First, to investigate the energy consumption of MCDI as function of water recovery, in Section 3.1, we feed NaCl solutions with different inlet concentrations (20, 40, 60, 80 and 100 mM) to the stack and desalinate each solution to half of its initial concentration (Fig. 4a) for a duration of 100 s in order to achieve 50% salt removal efficiency,

$$\eta = 1 - \frac{c_{in} - c_{eff}}{c_{in}},$$

where c_{in} is the influent salt concentration and c_{eff} is the effluent salt concentration. To achieve this aim, we manually tune the electrical current I_{ads} to a value that leads to $\eta = 50\%$. It turns out that for each of the cases, which have the same inlet salt concentration but different WRs, to reach $\eta = 50\%$, the required I_{ads}'s are the same (orange triangles in Fig. 4a). During the desorption step, in order to obtain different water recoveries (WR), we use 3 different desorption currents (I_{des}) which are exactly −1, −2 and −3 times the adsorption current, respectively, to increase WR from 50% to 63% and to 68% (see Fig. 4a). The desorption current is applied until the cell voltage drops to zero, while the water flow rate of the stack is kept at 30 mL/min (Fig. 4a). Second, in Section 3.2, the influence of varying water flow rate has been investigated based on a fixed water recovery of 50%. Three water flow rates (15, 30 and 60 mL/min) have been used. For the adsorption step (100 s), for all water flow rates, we use suitable I_{ads} to reach 50% removal efficiency, η. During the desorption step, electrical current for desorption, I_{des}, is set equal to $-I_{ads}$ (Fig. 4b), and thus at DE, the duration of the desorption step is the same as that of the adsorption step. Finally, in Section 3.3, in order to compare MCDI with RO, we desalinate each influent concentration to the so-called "palatable water level" (0.5 g TDS/L, ~8.6 mM NaCl) and to the freshwater limit (1 g TDS/L, ~17.2 mM NaCl) (Fig. 4c) [35]. For each of these two cases analyzed in Section 3.3, WR is set to 50%, and the durations of both the adsorption step and the desorption step are set to 120 s.

3. Results and discussion

In this section, we will show the energy consumption per ion removed as function of influent salt concentration for different water recovery and water flow rate, and we will show the fraction of energy which can be recovered during the ion-release step. Furthermore, we will also compare the energy consumption per m^3 freshwater produced by our MCDI stack with literature data of reverse osmosis.

3.1. Energy consumption for different water recoveries

In this section, we will discuss energy consumption of our MCDI system for different water recoveries. In this section, we change the water recovery by varying the desorption current, while the required adsorption current for any case with the same influent salt concentration turns out to be the same in order to reach 50% salt removal efficiency, η. When DE is reached, and in case that $I_{ads} = -I_{des}$, the duration of the adsorption step t_{ads} and that of the desorption step t_{des} will be the same, which result in a 50% WR. Likewise, if $-I_{des} > I_{ads}$, the duration of the desorption step will be shorter than that of the adsorption step, leading to a quicker desorption and a higher WR. In Fig. 5, we show results of energy consumption and energy recovery for WR ranging from 50% to 68% by varying the desorption current. It is shown in Fig. 5a that first of all, higher WR obviously leads to higher energy consumption per ion removed, which is in agreement with the conclusion in ref. [31]. Second, we also find that a higher influent salt concentration leads to higher energy costs per ion removed. Because the salt removal efficiency η is fixed at 50%, a higher influent salt concentration also means a higher total salt removal. In other words, for a given device, and a given water flow rate, removing more ions consumes more energy per ion when η is fixed. For instance in Fig. 5a ($\eta = 50\%$), the salt removal at 100 mM in a period of 100 s (~0.16 mmol/g electrode mass) is about five times the salt removal at 20 mM (~0.035 mmol/g electrode mass). Besides higher salt removal, the energy consumption per ion removed of desalinating 100 mM NaCl to 50 mM for 100 s (~48 kT) is 3.5 times that of desalinating 20 mM NaCl to 10 mM for 100 s (~14 kT).

Fig. 5b shows the percentage of energy that can be recovered during the ion desorption step related to the energy input during the ion-

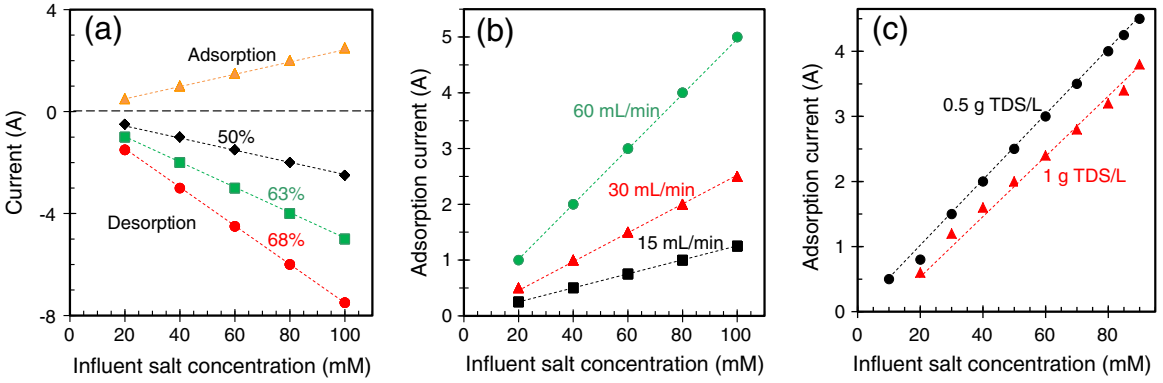

Fig. 4. Electrical current applied to achieve $\eta = 50\%$ (a) for different WR in Section 3.1, (b) for different water flow rate in Section 3.2, (c) for different effluent salt concentration in Section 3.3. In panel (a), I_{ads} is the same at one influent salt concentration for all water recoveries. In panels (b) and (c), $I_{ads} = -I_{des}$. Dashed lines serve to guide the eyes.

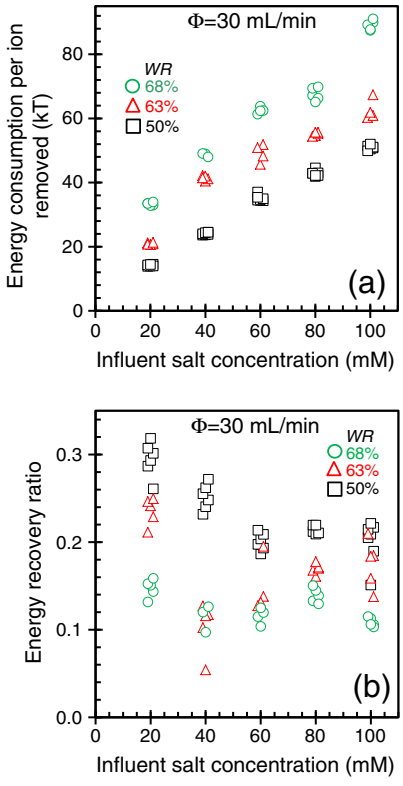

Fig. 5. Energy consumption per ion removed (a) and energy recovery (b) as a function of influent salt concentration. Different symbols represent different values of water recovery. Circles: 68%; triangles: 63%; squares: 50%. Experimental conditions are $\Phi = 30$ mL/min, $\eta = 50\%$, and $t_{ads} = 100$ s.

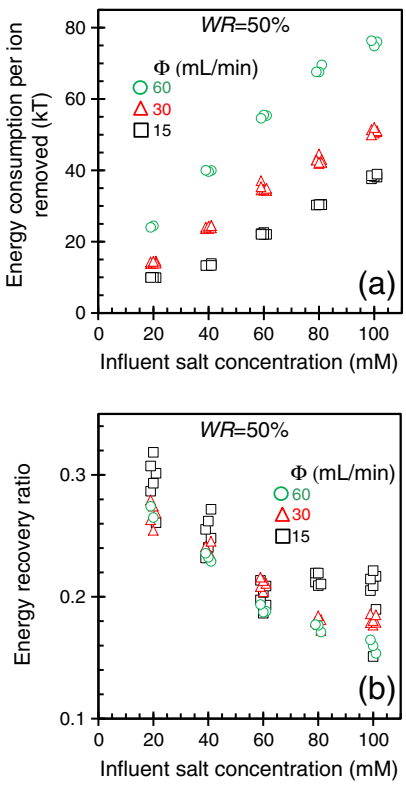

Fig. 6. Energy consumption per ion removed (a) and energy recovery (b) as a function of influent salt concentration. All data are for 50% water recovery. Different symbols represent different water flow rates in the stack. Squares: 15 mL/min; triangles: 30 mL/min; circles: 60 mL/min. Experimental conditions are $\eta = 50\%$, and $t_{ads} = t_{des} = 100$ s.

adsorption step. As can be seen from Fig. 5b, in order to reach 50% η, higher WR leads to lower energy recovery. This may be explained by the fact that to reach a higher WR, a higher desorption current is needed (Fig. 4a), which generates a higher ohmic drop. In the field of electrochemistry, the so-called "ohmic drop" is often used to describe the energy dissipated by internal resistances (see Fig. 3b). Table 2 shows the ohmic drop for values of WR in the same experimental setup with the influent concentration of 60 mM, where a higher WR leads to a higher Ohmic drop. Thus, because of higher desorption current used, more energy is required to overcome the internal resistances during the desorption step [31], and less energy can be recovered. The highest energy recovery is found when the influent salt concentration is 20 mM with a 50% WR, with a maximum value of 30% energy recovery, lower than the values given in Refs. [32] and [31].

3.2. Energy consumption for different water flow rates

In this section, the results of varying the water flow rate are presented. As can be seen in Fig. 6a, the energy consumption per ion removed increases quite linearly when the influent salt concentration is increased, which is similar to what we found in Fig. 5a. Another observation is that the energy consumption increases as the water flow rate is increased, which shows that to remove a given amount of salt ions, less energy is consumed at a lower water flow rate. Fig. 6b shows that when the flow rate is lower, the required electrical current to achieve 50% η is also lower. That means that when reversing the electrical current (changing from the ion adsorption step to the ion desorption step) a smaller Ohmic drop will be expected [31], which is reflected in a lower energy consumption per ion removed. Table 3 shows the Ohmic drop for the three water flow rates at $c_{in} = 40$ mM, indicating that a lower water flow rate leads to a lower Ohmic drop, leading to less energy lost in internal resistances. For the energy recovery, Fig. 6b shows that the water flow rate does not have a strong influence on the energy recovery. However, a clear trend can be found here that a lower influent salt concentration leads to a higher energy recovery, given the constraint that the η and the WR are both fixed at 50%.

3.3. Energy consumption for producing freshwater, and comparison with reverse osmosis

It is indubitable that the thermodynamic minimal energy required for desalination is independent of the type of separation process [7]. However, because of fundamental differences between desalination technologies, the energy required to remove a given amount of salt can vary significantly. To investigate the competitiveness of MCDI, here we compare its energy consumption per volume fresh water produced with the most prevalent technique, reverse osmosis (RO). For the energy consumption of RO, data are obtained from literature, see Table 4; and for comparison, a 13-cell MCDI unit is constructed consisting 26 electrodes ($\delta_e = 383$ μm, and $m_{tot} = 19.0$ g).

Table 2
Ohmic drop for WR of 50%, 63% and 68% of the influent salt concentration of 60 mM.

WR (%)	50	63	68
Ohmic drop (V)	0.77	1.63	1.94

Table 3
Ohmic drop for flow rate of 15, 30 and 60 mL/min at the influent salt concentration of 40 mM.

Flow rate (mL/min)	15	30	60
Ohmic drop (V)	0.77	0.81	1.29

Table 4
Examples of configurations of reverse osmosis plants. Feed water concentrations presented with ‡ are converted from ppm, and with † are converted from conductivity measurement (μS/cm). In this conversion, 1 ppm is assumed to be equal to 1 mg/L, and 1 μS/cm is assumed to be equal to 0.5 mg/L, according to Refs. [36,37]. "n/a" denotes "not available".

Location	Feed water concentration (g/L)	Capacity (m^3/d)	Energy consumption (kWh/m^3)	Water cost (US$/$m^3$)	Year of data access	Water recovery	Reference
Elhamarawien, Egypt	3.5‡	53	0.89	11.6	1986	n/a	[38]
White Cliffs, Australia	3.5‡	0.5	2	9	2003	n/a	[38]
Solar flow, Australia	5‡	0.4	1.86	10–12	1982	n/a	[38]
Conception del Oro, Mexico	3‡	0.71	6.9	n/a	1982	n/a	[38]
Mesquite, Nevada	3.5‡	1.5	1.38	3.6	2003	n/a	[38]
Denver, ITN, USA	1.6‡	1.5	1.4	6.5	2003	n/a	[39]
Hassi-Khebi, DZA	3.5‡	0.85	2.1	10	1987	n/a	[39]
Pine Hill, AUS	5.3‡	1.1	1.5	3.7	2008	n/a	[39]
Ksar Ghilene, TUN	3.5‡	7	2.1	6.5	2005	n/a	[39]
Heelat Ar Rakah, OMN	1.01‡	5	2.3	6.5	1999	n/a	[39]
Univ. of Almeria, ESP	3.36‡	8.09	2.5	2.5	1988	n/a	[39]
Coite-Pedreiras, BRA	1.2‡	6	3	12.8	2000	n/a	[39]
Seriwa, Perth, Aus	5.7‡	0.55	4.9	9.6	1982	n/a	[39]
Lampedusa, ITA	8‡	40	5.5	10.6	1990	n/a	[39]
VARI-RO, USA	7‡	3.6	2.4	9	1999	n/a	[39]
Baja California Sur, MEX	4‡	11.5	2.6	9.8	2005	n/a	[39]
Lipari, ITA	8‡	13.7	6.5	10.6	1991	n/a	[39]
Univ. of Athens, GRC	0.4‡	1000	7.7	2.8	2000	n/a	[39]
Cadarache, FRA	2†	15	0.7	n/a	1978	n/a	[40]
El Hamrawein, EGY	3†	216	1	n/a	1981	n/a	[41]
Maagan Michael, ISR	4‡	6.8	5	3	1997	n/a	[42]
Caple, Spain	6†	4000	1.72	0.29	2002	n/a	[43]
Vall D'Uixo, Spain	1.125†	7500	0.6	0.14	1997	n/a	[43]
Nules, Spain	1.529†	6000	0.83	0.17	2002	n/a	[43]
Cuevas de Almanzora, Spain	6.75†	25000	1.2	0.246	2003	n/a	[43]
Drenajes, Spain	6.25†	6000	1.2	0.3	1997	n/a	[43]
Terciario Alacanti Norte, Spain	1.75†	5000	1.55	0.36	2010	n/a	[43]
Citrico del Andevalo, Spain	0.6†	1200	0.86	0.14	2007	90%	[43]
Sidmed, Spain	0.4†	750	1.2	0.22	1995	n/a	[47]
Xeresa Golf, Spain	1.7†	5000	0.85	0.29	2003	n/a	[43]
Alicante University, Spain	3.2†	450	1.1	0.22	1996	n/a	[43]
AENA, Spain	0.9†	200	1	0.18	1999	n/a	[43]
San Vicente del Raspeig, Spain	4.25†	100	1	0.25	1998	n/a	[43]
Gaza Strip area	1.625	60	1.35	n/a	1993	75%	[44]
Ceara, Brazil	1.2‡	6	3.03	n/a	2000	27%	[45]
Gran Canaria, Spain	3.36‡	0.8	2.48	n/a	1988	26-64%	[45]
Algeria	3‡	22.4-26.4	2.075	n/a	1988	24-40.7%	[45]
Egypt	4.4‡	0.24	0.89	n/a	1986	51%	[46]
Jordan	1.7‡	0.22-1.27	1.9	n/a	2011	22%	[46]
Kerkennah Islands, Tunisia	3.7	3300	1.1	n/a	2003	75%	[47]

A series of experiments are performed on the 13-cell MCDI stack, and in all cases, we use NaCl as the influent salt solution. We flow solutions with a concentration ranging from 0.4 to 5.2 g/L TDS (20 to 90 mM NaCl, 1 g/L TDS = 17.1 mM) into the stack, and desalinate them either to 0.5 g/L TDS (8.6 mM NaCl) or to 1 g/L TDS (17.2 mM NaCl), in both cases using the CC-RCD mode ($I_{ads} = -I_{des}$, desorption until V_{cell} is back to zero), where the duration of both the adsorption and the desorption step is 120 s (water recovery WR = 50%, the water flow rate is 30 mL/min per stack, and the required electrical adsorption current I_{ads} to achieve this aim is given in Fig. 4c). The two freshwater concentration levels defined above represent palatable drinking water (with good taste) and the limit of drinking water, respectively [35]. As presented in Fig. 7, the majority of data for RO systems shows energy consumption below 2 kWh/m^3 within the whole range of concentrations. In case of MCDI, if the product salinity is 1 g/L TDS (diamonds in Fig. 7), and when the influent salt content is below ~3 g/L, MCDI can be advantageous over RO. However if even purer water (~0.5 g/L TDS) has to be produced, the energy consumption for each value of the influent salt concentration is nearly doubled. This result suggests that MCDI becomes competitive only if the influent salt concentration is below 2 g/L TDS.

Note that in this study the pumping energy of MCDI is not included, but unlike RO, MCDI does not need a high pressure to press water through the membrane. Instead, water is transported only in between the two ion-exchange membranes, which does not require a substantial pressure drop between the influent and the effluent of the stack. In the case of our experimental setup, we have measured the pressure drop across the stack, which is $p \sim 0.1$ bar. The required minimum pumping energy per cycle can be thus calculated as

$$E_{pumping} = \Phi \cdot p \cdot t_{cycle,} \quad (4)$$

where Φ is the flow rate (in this case 30 mL/min), $E_{pumping}$ is the pumping energy consumption per cycle, and p is the pressure drop

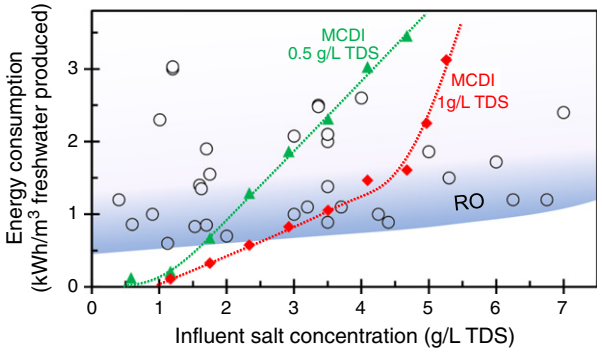

Fig. 7. Comparison of energy consumption between MCDI and reverse osmosis. Triangles: energy consumption of MCDI to bring salt concentration to the level of 0.5 g/L TDS (~ upper limit for palatable drinking water). Diamonds: energy consumption of MCDI to reduce salt concentration to 1 g/L TDS (~upper limit for drinking water). Circles: RO data. The data sources for RO are listed in Table 2. Dashed lines are to guide the eyes.

across the stack. Thus, $E_{pumping}$ is 1.2 J/cycle. Since in one cycle the fresh water production is given by $V_{fresh} = \Phi \cdot t_{cycle} \cdot WR = 60$ mL, the pumping energy per m^3 fresh water produced is $E_{pumping}/V_{fresh} = 5.5 \cdot 10^{-3}$ kWh. Compared to the electrical energy requirement, see Fig. 7, the pumping energy required for producing 1 m^3 fresh water is rather small.

Another remark is that our system is not optimized for industrial objectives, and it seems likely that the energy consumption can be further reduced by optimizing the system and reducing the electronic resistances. Thus, MCDI has the potential to compete with RO to desalinate brackish water. Future research on MCDI could focus on reducing the energy consumption, which is among the most relevant issues towards application.

4. Conclusions

In conclusion, in this work, we demonstrated a modified method for data analysis of salt adsorption and energy consumption for the capacitive deionization process, a method which gives a more realistic estimate of the salt removal capacity and the energy consumption. Furthermore, we showed that when the removal efficiency is fixed, operation of MCDI system in the CC-RVD mode consumes more energy when the water recovery or water flow rate is increased. Finally, we present data for the specific energy consumption as function of influent salt concentration in our lab-scale experimental setup, and compared these data with RO data reported in literature for full-scale RO desalination plants. It is found that MCDI works better in the lower concentration range, roughly below 60 mM.

Acknowledgement

This work was performed in the TTIW-cooperation framework of Wetsus, Centre of Excellence for Sustainable Water Technology, Leeuwarden, the Netherlands. Wetsus is funded by the Dutch Ministry of Economic Affairs, the European Union Regional Development Fund, the Province of Friesland, the City of Leeuwarden, and the EZ/Kompas program of the 'Samenwerkingsverband Noord-Nederland'. We thank the participants of the theme "Capacitive Deionization" for their involvement in this research.

References

[1] I.A. Shiklomanov, Appraisal and assessment of world water resources, Water Int. 25 (2000) 11–32.
[2] T. Buerkle, Making every drop count, Food and Agriculture Organization of the United Nations, 2007, (http://www.fao.org/newsroom/en/news/2007/1000494/index.html).
[3] A. Cipollina, Seawater desalination: conventional and renewable energy processes, Springer, Berlin, 2009.
[4] T.Y. Cath, A.E. Childress, M. Elimelech, Forward osmosis: principles, applications, and recent developments, J. Membr. Sci. 281 (2006) 70–87.
[5] A. Mani, M.Z. Bazant, Deionization shocks in microstructures, Phys. Rev. E 84 (2011) 061504.
[6] A. Subramani, M. Badruzzaman, J. Oppenheimer, J.G. Jacangelo, Energy minimization strategies and renewable energy utilization for desalination: a review, Water Res. 45 (2011) 1907–1920.
[7] S. Porada, R. Zhao, A. van der Wal, V. Presser, P.M. Biesheuvel, Review on the science and technology of water desalination by capacitive deionization, Prog. Mater. Sci. 58 (2013) 1388–1442.
[8] B.B. Arnold, G.W. Murphy, Studies on electrochemistry of carbon and chemically modified carbon surfaces, J. Phys. Chem. 65 (1961) 135–138.
[9] M. Haro, G. Rasines, C. Macias, C.O. Ania, Stability of a carbon gel electrode when used for the electro-assisted removal of ions from brackish water, Carbon 49 (2011) 3723–3730.
[10] E. Avraham, M. Noked, I. Cohen, A. Soffer, D. Aurbach, The dependence of the desalination performance in capacitive deionization processes on the electrodes PZC, J. Electrochem. Soc. 158 (2011) 168–173.
[11] S.-J. Seo, H. Jeon, J.K. Lee, G.-Y. Kim, D. Park, H. Nojima, J. Lee, S.-H. Moon, Investigation on removal of hardness ions by capacitive deionization (CDI) for water softening applications, Water Res. 44 (2010) 2267–2275.
[12] L. Zou, L. Li, H. Song, G. Morris, Improving the capacitive deionisation performance by optimising pore structures of the electrodes, Water Sci. Technol. 61 (2010) 1227–1233.
[13] M.E. Suss, T.F. Baumann, W.L. Bourcier, C.M. Spadaccini, K.A. Rose, J.G. Santiago, M. Stadermann, Capacitive desalination with flow-through electrodes, Energy Environ. Sci. 5 (2012) 9511–9519.
[14] T. Humplik, J. Lee, S.C. O'Hern, B.A. Fellman, M.A. Baig, S.F. Hassan, M.A. Atieh, F. Rahman, T. Laoui, R. Karnik, E.N. Wang, Nanostructured materials for water desalination, Nanotechnology 22 (2011) 292001.
[15] G. Wang, Q. Dong, Z. Ling, C. Pan, C. Yu, J. Qiu, Hierarchical activated carbon nanofiber webs with tuned structure fabricated by electrospinning for capacitive deionization, J. Mater. Chem. 22 (2012) 21819–21823.
[16] P.M. Biesheuvel, Y. Fu, M.Z. Bazant, Electrochemistry and capacitive charging of porous electrodes in asymmetric multicomponent electrolytes, Russ. J. Electrochem. 48 (2012) 580–592.
[17] S. Porada, M. Bryjak, A. Van Der Wal, P.M. Biesheuvel, Effect of electrode thickness variation on operation of capacitive deionization, Electrochim. Acta 75 (2012) 148–156.
[18] S. Porada, L. Borchardt, M. Oschatz, M. Bryjak, J.S. Atchison, K.J. Keesman, S. Kaskel, P.M. Biesheuvel, V. Presser, Direct prediction of the desalination performance of porous carbons for capacitive deionization, Energy Environ. Sci. (2013), http://dx.doi.org/10.1039/C3EE42209G(in press).
[19] R. Zhao, M. van Soestbergen, H.H.M. Rijnaarts, A. van der Wal, M.Z. Bazant, P.M. Biesheuvel, Time-dependent ion selectivity in capacitive charging of porous electrodes, J. Colloid Interface Sci. 384 (2012) 38–44.
[20] H. Li, Y. Gao, L. Pan, Y. Zhang, Y. Chen, Z. Sun, Electrosorptive desalination by carbon nanotubes and nanofibres electrodes and ion-exchange membranes, Water Res. 42 (2008) 4923–4928.
[21] J.-B. Lee, K.-K. Park, H.-M. Eum, C.-W. Lee, Desalination of a thermal power plant wastewater by membrane capacitive deionization, Desalination 196 (2006) 125–134.
[22] Y.-J. Kim, J.-H. Choi, Improvement of desalination efficiency in capacitive deionization using a carbon electrode coated with an ion-exchange polymer, Water Res. 44 (2010) 990–996.
[23] C.Y. Nie, Y.K. Zhan, L.K. Pan, H.B. Li, Z. Sun, Electrosorption of different cations and anions with membrane capacitive deionization based on carbon nanotube/nanofiber electrodes and ion-exchange membranes, Desalin. Water Treat. 30 (2011) 266–271.
[24] J.-Y. Lee, S.-J. Seo, S.-H. Yun, S.-H. Moon, Preparation of ion exchanger layered electrodes for advanced membrane capacitive deionization (MCDI), Water Res. 45 (2011) 5375–5380.
[25] B.-H. Park, Y.-J. Kim, J.-S. Park, J. Choi, Capacitive deionization using a carbon electrode prepared with water-soluble poly(vinyl alcohol) binder, J. Ind. Eng. Chem. 17 (2011) 717–722.
[26] R. Zhao, P.M. Biesheuvel, A. Van der Wal, Energy consumption and constant current operation in membrane capacitive deionization, Energy Environ. Sci. 5 (2012) 9520–9527.
[27] T.J. Welgemoed, C.F. Schutte, Capacitive delonization technology (TM): an alternative desalination solution, Desalination 183 (2005) 327–340.
[28] Y. Oren, Capacitive delonization (CDI) for desalination and water treatment—past, present and future (a review), Desalination 228 (2008) 10–29.
[29] M. Elimelech, W.A. Phillip, The future of seawater desalination: energy, technology, and the environment, Science 333 (2011) 712–717.
[30] M.A. Anderson, A.L. Cudero, J. Palma, Capacitive deionization as an electrochemical means of saving energy and delivering clean water. Comparison to present desalination practices: will it compete? Electrochim. Acta 55 (2010) 3845–3856.
[31] P. Długołęcki, A. van der Wal, Energy recovery in membrane capacitive deionization, Environ. Sci. Technol. 47 (2013) 4904–4910.
[32] O.N. Demirer, R.M. Naylor, C.A. Rios Perez, E. Wilkes, C. Hidrovo, Energetic performance optimization of a capacitive deionization system operating with transient cycles and brackish water, Desalination 314 (2013) 130–138.
[33] R. Zhao, O. Satpradit, H.H.M. Rijnaarts, P.M. Biesheuvel, A. van der Wal, Optimization of salt adsorption rate in membrane capacitive deionization, Water Res. 47 (2013) 1941–1952.
[34] S. Porada, B.B. Sales, H.V.M. Hamelers, P.M. Biesheuvel, Water desalination with wires, J. Phys. Chem. Lett. 3 (2012) 1613–1618.
[35] Health implications of increased salinity of drinking water, Department of Health, Government of South Australia, 2008, (http://www.dh.sa.gov.au/pehs/PDF-files/ph-factsheet-water-salinity.pdf).
[36] AppsLabrotaries, http://appslabs.com.au/salinity.htm.
[37] Broads Authority, http://www.broads-authority.gov.uk/broads/live/managing/rivers-and-broads/broads-water-quality-partnership/Guide_to_the_relatioinship_between_salinity_measures.pdf.
[38] A.A. Al-Karaghouli, L.L. Kazmerski, Renewable Energy Opportunities in Water Desalination, in: M. Schorr (Ed.), Desalination, Trends and Technologies, InTech, 2011.
[39] A. Ghermandi, R. Messalem, Solar-driven desalination with reverse osmosis: The state of the art, Desalin. Water Treat. 7 (2009) 285–296.
[40] A. Maurel, Dessalement et energies nouvelles, Desalination 31 (1979) 489–499.
[41] J.J. Libert, A. Maurel, Desalination and renewable energies-a few recent developments, Desalination 39 (1981) 363–372.
[42] D. Weiner, D. Fisher, E.J. Moses, B. Katz, G. Meron, Operation experience of a solar- and wind-powered desalination demonstration plant, Desalination 137 (2001) 7–13.
[43] D.Z. Martinesz, C.G.G. Soto, R.B. Candel, Experiences on desalination of different brackish water, IDA World Congress, Atlantis, The Palm-Dubai, UAE, 2009.
[44] V. Frenkel, T. Gourgi, Brackish water RO desalination plant in the Gaza Strip, Desalination 101 (1995) 47–50.
[45] P.C.M. de Carvalho, D.B. Riffel, C. Freire, F.F.D. Montenegro, The Brazilian experience with a photovoltaic powered reverse osmosis plant, Prog. Photovolt. Res. Appl. 12 (2004) 373–385.
[46] H. Qiblawey, F. Banat, Q. Al-Nasser, Performance of reverse osmosis pilot plant powered by Photovoltaic in Jordan, Renew. Energy 36 (2011) 3452–3460.
[47] K. Fethi, Optimization of energy consumption in the 3300 m3/d RO Kerkennah plant, Desalination 157 (2003) 145–149.